Support information

Ni single atom catalyst with high Ni-N_X content for efficient electrocatalytic reduction of CO_2

Yuting Feng [a], Qing Mao[*,a] , Hongbin Yang[*,b], Wei Zhou [a], Dengye Yang[a], Yanfei Gao,[d]

[a] School of Chemical Engineering, Dalian University of Technology, Dalian 116024, China

[b] School of Materials Science and Engineering, Suzhou University of Science and Technology, Suzhou 215011, China

[c] Shanghai Triumph Energy Conservation Engineering Co., Ltd, Shanghai 200333, China

[*]Corresponding Author: Qing Mao, Hongbin Yang

Supplementary Note 1: Product analysis and turnover frequency calculations

The gas-phase products of the CO_2RR were quantified using a gas chromatography (GC7900 Techcomp) system equipped with a nickel catalysis transition furnace, a thermal conductivity detector (TCD), and a flame ionization detector (FID). Gas bags were used to collect gas products at each potential for quantitative detection. The details for Faradaic efficiency calculations are shown in Supplementary Note 1. Liquid products were quantified using ^1H NMR spectroscopy (Bruker Avance II 400) by a water peak pressing procedure, in which dimethyl sulfoxide was chosen as the reference.

The Faradaic efficiencies (FE) of products in CO_2RR were calculated from the areas of the gas chromatography as indicated below:

$$FE(\%) = \frac{J_{co}}{J_{tot}} \times 100\ \% = \frac{n_{co} \times N \times F}{I \times t} \times 100\ \% \qquad \text{(Eq. S1)}$$

The Faradaic efficiencies (*FE*) of products in CO_2 pulsed electroreduction were calculated as indicated below:

$$FE(\%) = \frac{J_{co}}{J_{tot}} \times 100\ \% = \frac{n_{co} \times N \times F}{I \times t} \times 100\ \% \qquad \text{(Eq. S2)}$$

where

J_{co}: partial current density toward CO production;

J_{tot}: total current density;

N: number of electrons transferred, which is 2 for CO;

n_{co}: the production rate of CO;

F: Faradaic constant, 96485 $C \cdot mol^{-1}$

Turnover frequency (*TOF*) was estimated based on the following equation:

$$TOF\left(h^{-1}\right)=\frac{CO_{molecule/h}}{Metal_{atom}}=\frac{I\cdot t\cdot FE_{CO}\cdot M_M}{n\cdot m_{catalyst}\cdot w_M\cdot F} \qquad \text{(Eq. S3)}$$

where

$CO_{molecule/h}$: the number of CO molecules produced in 1 h;

$Metal_{atom}$: the number of active metal atoms in the catalyst;

J: the total current density of CO_2RR at a specific potential;

t: reaction time, 1 h (3600 s);

FE_{CO}: Faradaic efficiency of CO;

M_M: relative molecular mass of metal;

n: the number of transferred electrons required to produce a CO molecule;

$m_{catalyst}$: the quality of the catalyst in the reaction;

w_M: the mass fraction of active metal in the catalyst;

Supplementary Note 2: Thermodynamic calculations

Assuming that the individual Ni atoms in Ni/NC-x are the active sites in the CO_2 to CO electroreduction process, Table S1 lists the reaction rate equations corresponding to the elementary reaction steps (Table 1, E(1) ~ E(4)). The control equations are listed in Table S2. Here, r is the elementary reaction rate [$mol \cdot m^{-2} \cdot s^{-1}$], K is the reaction rate constant [$mol \cdot m^{-2} \cdot s^{-1}$], c is the concentration [$mol \cdot m^{-3}$], and θ is coverage, α is the symmetry coefficient, η is the overpotential [V], R is the gas constant [$J \cdot mol^{-1} \cdot K^{-1}$], T is the temperature [K]; θ subscripts CO_2 and COOH represent the intermediates $*CO_2$ and *COOH, respectively; c subscripts CO_2 and HCO_3 represent the reactant CO_2 and electrolyte $KHCO_3$, respectively.

Table S1. Reaction rate equations for the CO_2 electroreduction on the Ni/NC-x

$$r_1 = K_{101}\left(1-\theta_{CO_{2,ads}}-\theta_{COOH_{ads}}-\theta_{CO_{ads}}\right)\left(\frac{C_{CO_2}}{C^{\Theta}}\right) \quad \text{(TS1.1)}$$

$$r_{-1} = K_{102}\cdot\theta_{CO_{2,ads}} \quad \text{(TS1.2)}$$

$$r_2 = K_{201}\theta_{CO_{2,ads}}\left(\frac{C_{CO_2}}{C^{\Theta}}\right)\exp\left(\frac{\alpha F\eta}{RT}\right) \quad \text{(TS1.3)}$$

$$r_{-2} = K_{202}\cdot\theta_{COOH_{ads}}\left(\frac{C_{HCO_3^-}}{C^{\Theta}}\right)\cdot\exp\left(-\frac{(1-\alpha)F\eta}{RT}\right) \quad \text{(TS1.4)}$$

$$r_3 = K_{301}\cdot\theta_{COOH_{ads}}\left(\frac{C_{HCO_3^-}}{C^{\Theta}}\right)\cdot\exp\left(\frac{\alpha F\eta}{RT}\right) \quad \text{(TS1.5)}$$

$$r_{-3} = K_{302}\cdot\theta_{CO}\left(\frac{C_{HCO_3^-}}{C^{\Theta}}\right)\cdot\exp\left(-\frac{(1-\alpha)F\eta}{RT}\right) \quad \text{(TS1.6)}$$

$$r_4 = K_{401}\cdot\theta_{CO_{ads}} \quad \text{(TS1.7)}$$

$$r_{-4} = K_{402}\cdot\left(1-\theta_{CO_{2,ads}}-\theta_{COOH_{ads}}-\theta_{CO_{ads}}\right)\left(\frac{P_{co}}{P^{\Theta}}\right) \quad \text{(TS1.8)}$$

Table S2. Control equations for the CO_2 electroreduction on the Ni/NC-x

$C_{CO_{2,suf}} \frac{d\theta_{CO_2}}{dt} = r_1 - r_{-1} - r_2 + r_{-2}$	(TS2.1)
$C_{COOH_{suf}} \frac{d\theta_{COOH}}{dt} = r_2 - r_{-2} - r_3 + r_{-3}$	(TS2.2)
$C_{COOH_{suf}} \frac{d\theta_{COOH}}{dt} = r_2 - r_{-2} - r_3 + r_{-3}$	(TS2.3)
$C_{dl} \frac{dE}{dt} = j(t) - \left[(r_2 - r_{-2}) + (r_3 - r_{-3}) \right] \cdot F / n$	(TS2.4)

The kinetics parameters (**Table S3**) are obtained by fitting the four-step CO_2RR kinetics model with steady state internal resistance (IR) corrected CO_2RR performance (IR corrected potential as independent variable and CO partial current densities as dependent variable) by means of a global optimization method, which is composed of a random search using genetic algorithm and a local optimization employing trust-region-reflective algorithm, that was reported by our previous publications [1,2].

[1] Qing Mao, Ulrike Krewer, Electrochimica Acta, 2013,103:188-198

[2] Qing Mao, Ulrike Krewer, Electrochimica Acta, 2012, 68:60-68

Table S3. Reaction kinetic constants of the four step CO_2RR

	Ni/NC-0	Ni/NC-2:1
K_{101}	2.13×10^{11}	1.06×10^{10}
K_{102}	3.32×10^{10}	1.59×10^{06}
K_{201}	3.72×10^{-05}	1.69×10^{-03}
K_{202}	5.59×10^{08}	9.09×10^{09}
K_{301}	1.70×10^{03}	3.12×10^{02}
K_{302}	1.83×10^{06}	4.54×10^{05}
K_{401}	9.48×10^{06}	4.07×10^{07}
K_{402}	3.75×10^{-09}	3.47×10^{-05}

The thermodynamic energy barrier can be calculated from standard free energy of formation ΔG_f° values of the reactants and products involved in the CO_2RR, which is the sum of the energy barriers of each elementary reaction. This relation is expressed by formula Eq. S4:

$$\Delta G = \Delta G_1 + \Delta G_2 + \Delta G_3 + \Delta G_4 \quad \text{(Eq. S4)}$$

The numerical relationship between the binding energy and the kinetic constant of each intermediate in the reaction process can be determined according to arrhenius equation. Therefore, the kinetic constant and the thermodynamic energy barrier are explicitly coupled in numerical form. Then the thermodynamic energy barrier of each intermediate in the reaction process can be simulated by Eq. S5

$$\Delta G = -RT \ln K^{\Theta} \quad \text{(Eq. S5)}$$

Supplementary Note 3: Experimental details

Electrode preparation for the H-cell

In a typical procedure, 10 mg of Ni/NC-x catalysts, and 40 μL of 5 wt. % Nafion solution (in ethanol/water) were dispersed in a 960 μL of mixture of water and isopropanol (volume ratio=1:1) to form a homogeneous ink by 60 min of ultrasonication. Subsequently, 100 μL of the ink were loaded onto a carbon paper electrode (AvCarb P75T, 1×1 cm^2) to obtain a catalyst loading of 1 mg/cm^2.

Electrode preparation for flow cell

Preparation of GDE: After sonication of 10 mg XC-72 and 250 μL anhydrous ethanol for 10 minutes, 250 μL of 10 wt% PTFE was added, stirred well, and then the mixture was brushed onto carbon paper. Finally, the carbon paper was baked at 340 ℃ for 1 hour.

Preparation of catalyst ink: 10 mg catalyst was added to 100 μL deionized water and ultrasonicated for 20 min, followed by the addition of 95 μL anion exchange resin mixture (6 mg of anion exchange resin dissolved in 95 mL anhydrous ethanol and 95 mL acetone), and the resulting ink was brushed onto GDE (2×2 cm^2) with a loading of 2 mg/cm^2.

Supplementary Figures and Tables

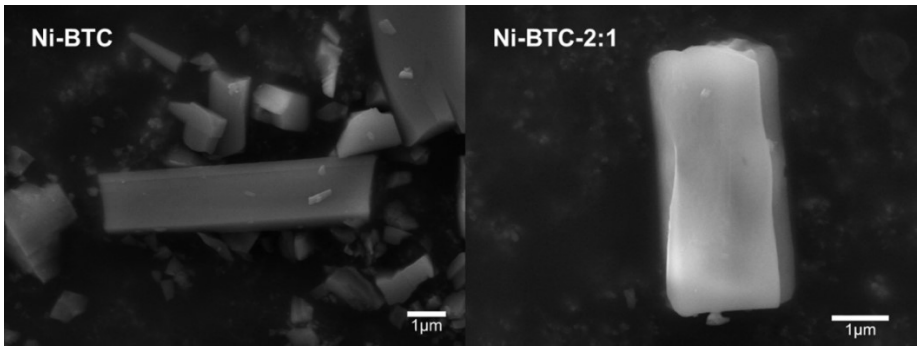

Figure S1. SEM image of Ni-BTC-0 and Ni-BTC-2:1, scale bar 1μm

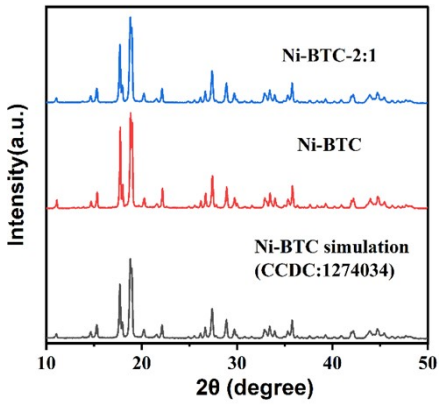

Figure S2. PXRD patterns of Ni-BTC and Ni-BTC-2:1

The hydrothermal synthesis of Ni-BTC was achieved using nickel chloride hexahydrate and homobenzoic acid in a dimethylformamide (DMF) medium. The resulting Ni-based metal-organic framework (MOF) exhibits a regular rectangular morphology and possesses a well-suited pore structure. The incorporation of polyvinylpyrrolidone (PVP) during the hydrothermal process enables the effective encapsulation of PVP within the MOF, without compromising the surface morphology or the physical phase integrity of Ni-BTC.

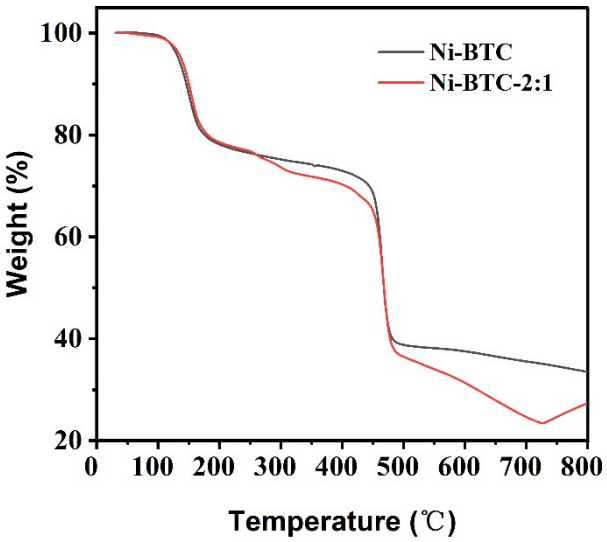

Figure S3. Thermogravimetric analysis (TGA) curves of Ni-BTC (black) and Ni-BTC-2:1 (red) measured in Ar atmosphere

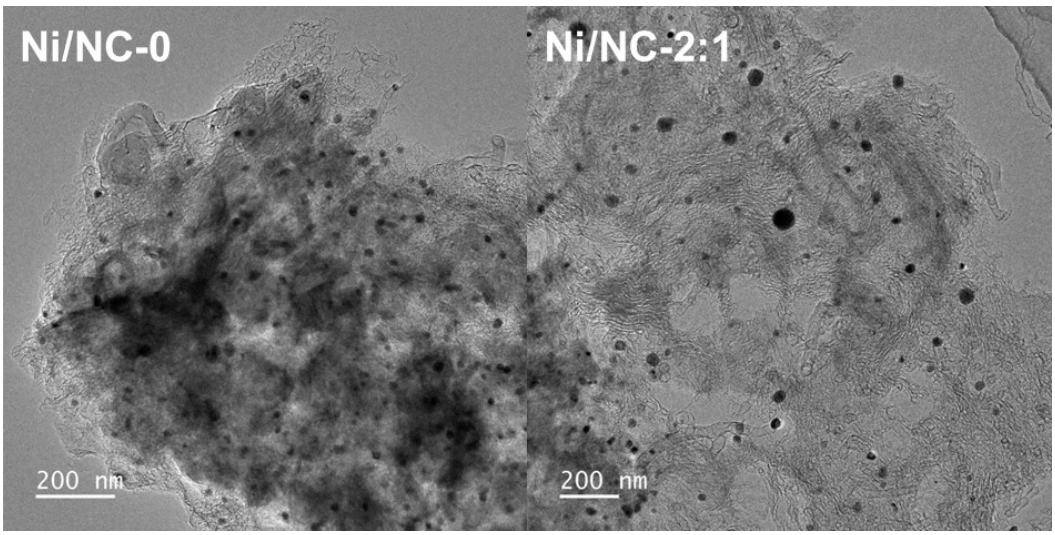

Figure S4. TEM image of Ni/NC-0 and Ni/NC-2:1

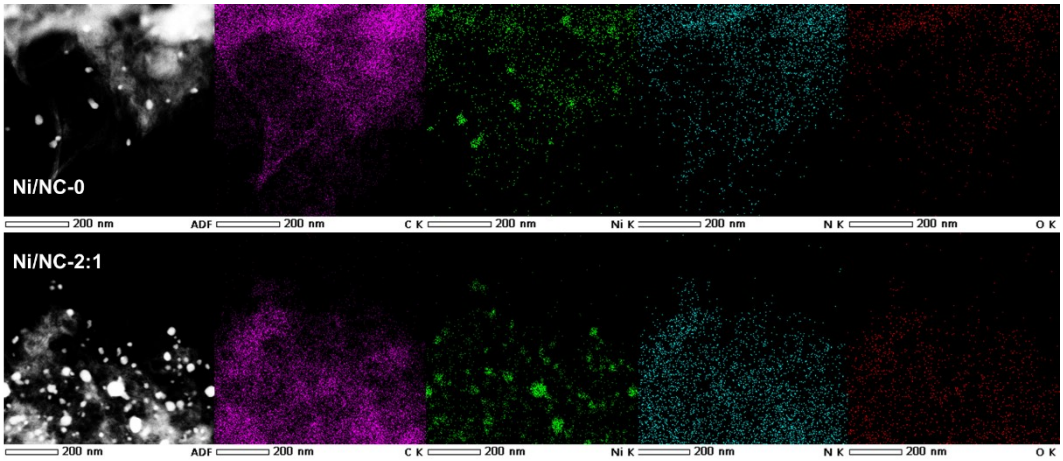

Figure S5. Elemental mappings of Ni/NC-0

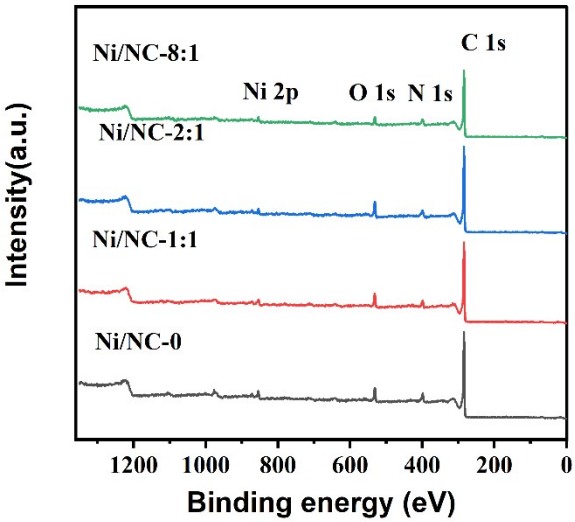

Figure S6. XPS survey of Ni/NC-0, Ni/NC-1:1, Ni/NC-2:1 and Ni/NC-8:1

Table S4. Ni contents in various catalysts determined by ICP-AES and XPS

Content	Ni/NC-0	Ni/NC-1:1	Ni/NC-2:1	Ni/NC-8:1
ICP-AES (%(wt))	4.64%	5.96%	5.12%	5.34%
XPS (%(at))	1.92%	1.66%	1.68%	1.42%

Table S5. XPS N1s element analysis results

Catalyst	Pyridinic N	Ni-N	Pyrrolic N	Graphitic N	Oxidized N
Ni/NC-0	48.11%	7.76%	16.49%	15.11%	12.53%
Ni/NC-1:1	47.86%	12.25%	15.43%	15.59%	8.86%
Ni/NC-2:1	46.8%	15.36%	13.74%	13.4%	10.71%
Ni/NC-8:1	48.7%	10.47%	16.61%	15.09%	9.13%

Table S6. The nitrogen adsorption/desorption measurement results of various catalysts

Samples	Ni/NC-0	Ni/NC-1:1	Ni/NC-2:1	Ni/NC-8:1
BET surface area($m^2 \cdot g^{-1}$)	196.25	194.85	176.82	179.32
Pore volume($cm^3 \cdot g^{-1}$)	0.44	0.48	0.44	0.41

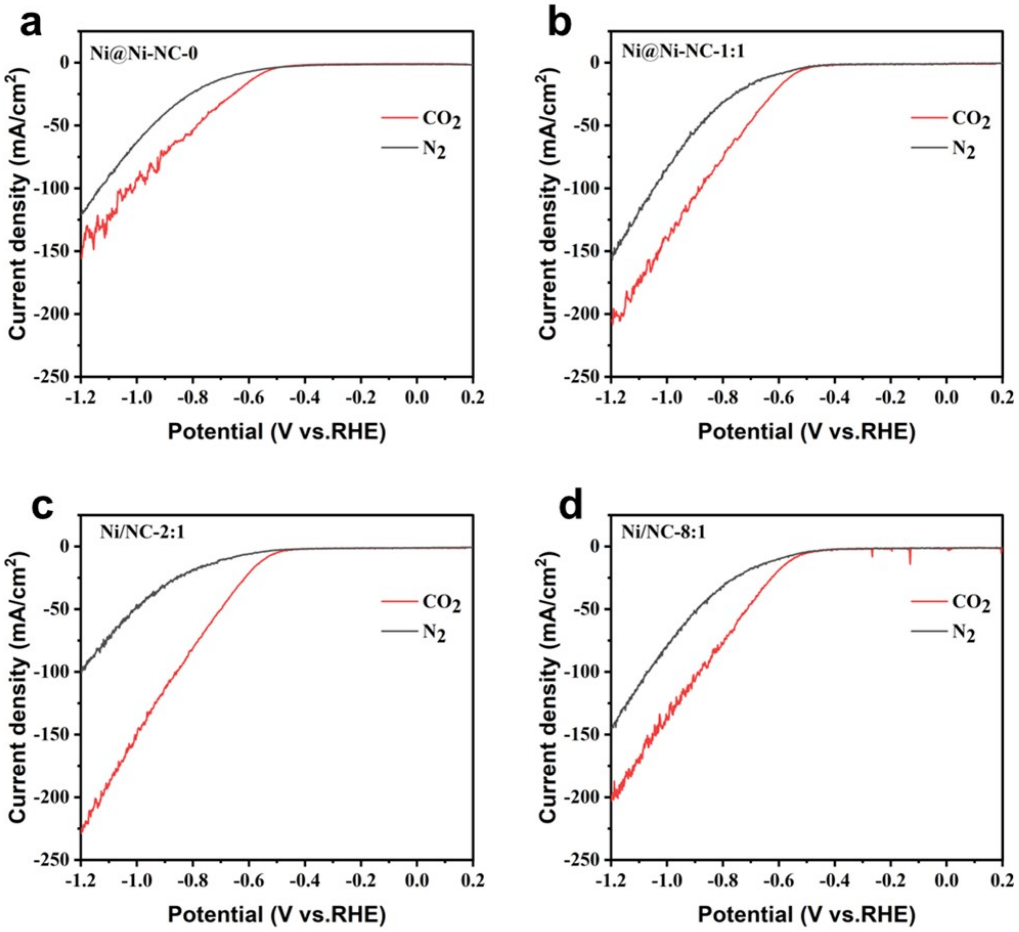

Figure S7. LSV of Ni/NC-x in CO_2-saturated and N_2-saturated electrolytes

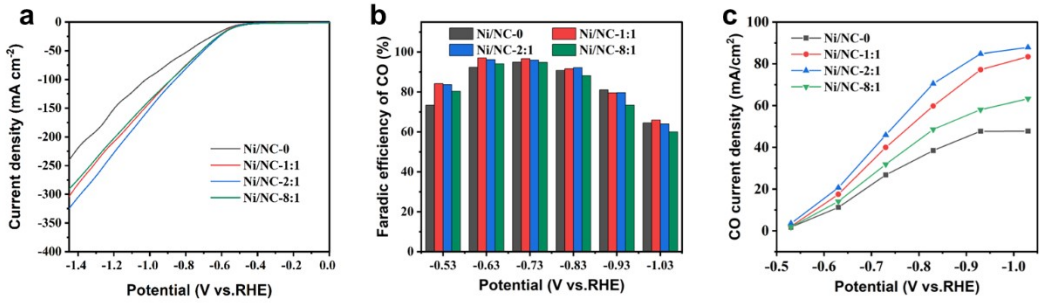

Figure S8. (a) LSV, (b) CO Faradic efficiency and (c) CO current density of Ni/NC-x in CO_2-saturated electrolytes

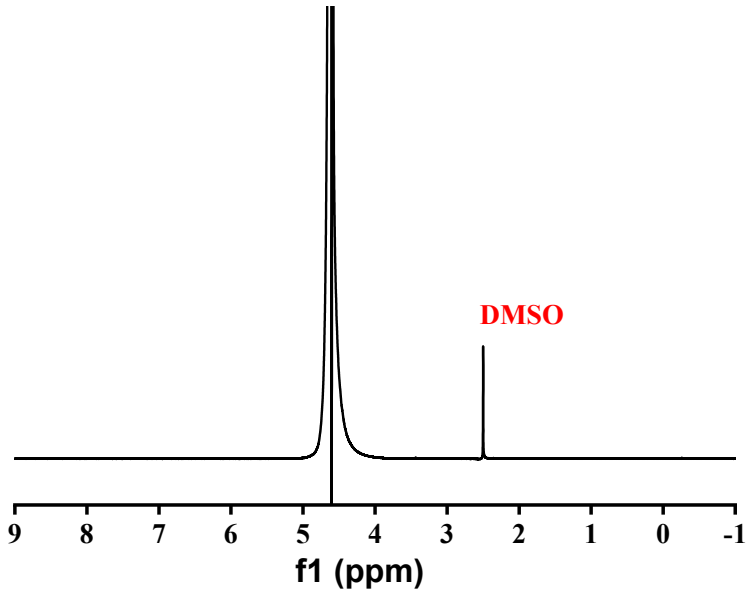

Figure S9. ^{1}H nuclear magnetic resonance (NMR) spectra of the electrolyte after 30 mins CO_2 reduction electrolysis at -0.73 V vs. RHE for Ni/NC-2:1.

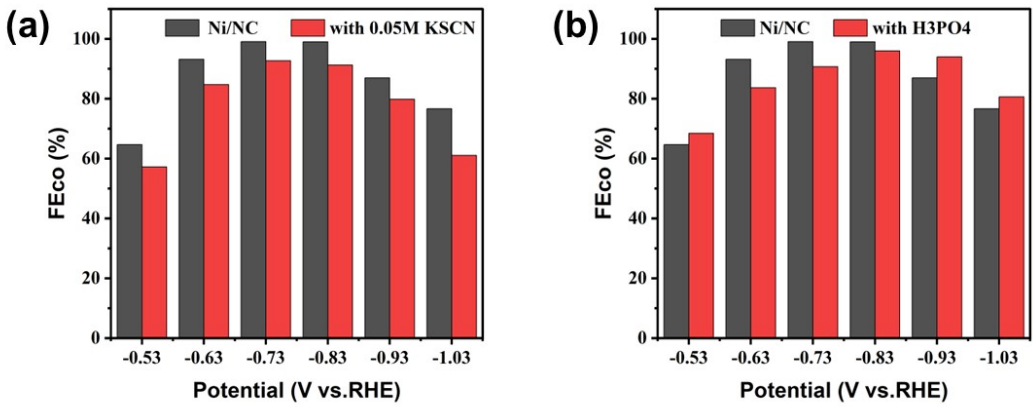

Figure S10. FE_{CO} of Ni/NC from the CO_2RR in CO_2-saturated 0.5 M $KHCO_3$ without and with 0.05M KSCN. (e) FE_{CO} of Ni/NC from the CO_2RR in CO_2-saturated 0.5 M $KHCO_3$ electrolyte without and with 0.1 M H_3PO_4 treatment

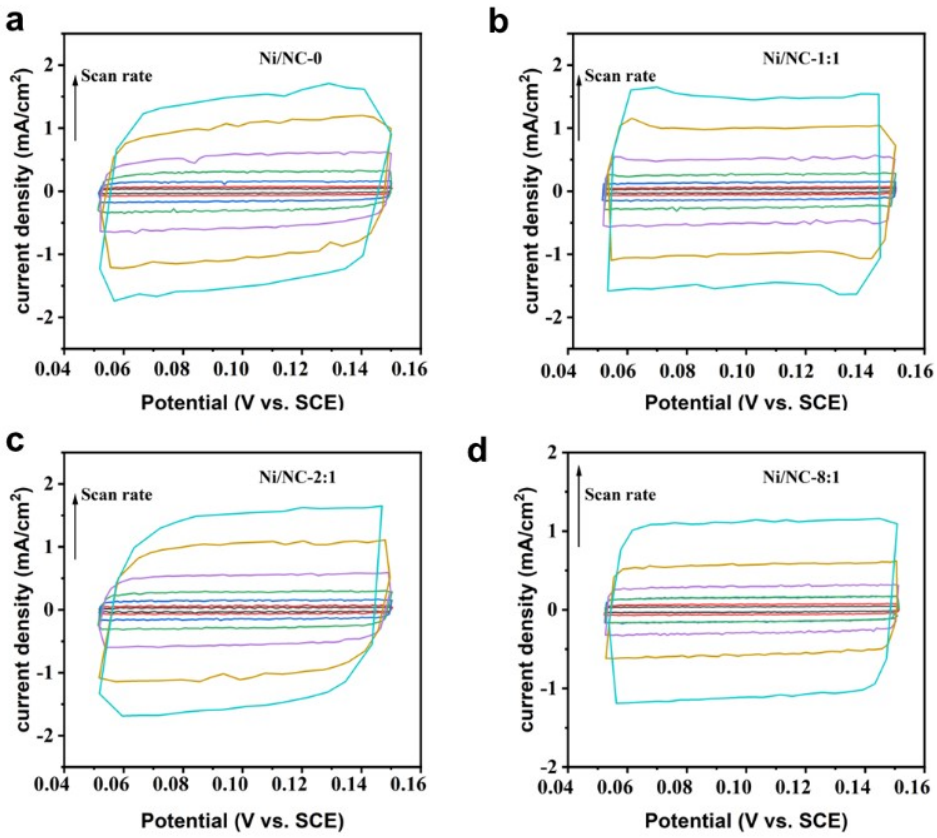

Figure S11. Cyclic voltammograms of the (a) Ni/NC-0, (b) Ni/NC-1:1, (c) Ni/NC-2:1 and (d) Ni/NC-8:1 recorded between 0.05-0.15V vs. RHE at the different sweep rate in CO_2-saturated 0.5 M $KHCO_3$ electrolyte.

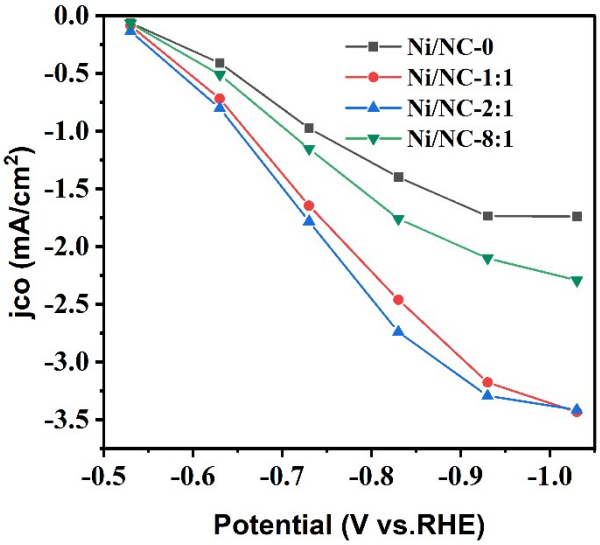

Figure S12. ECSA-normalizing CO current densities of Ni/NC-0, Ni/NC-1:1, Ni/NC-2:1 and Ni/NC-8:1.

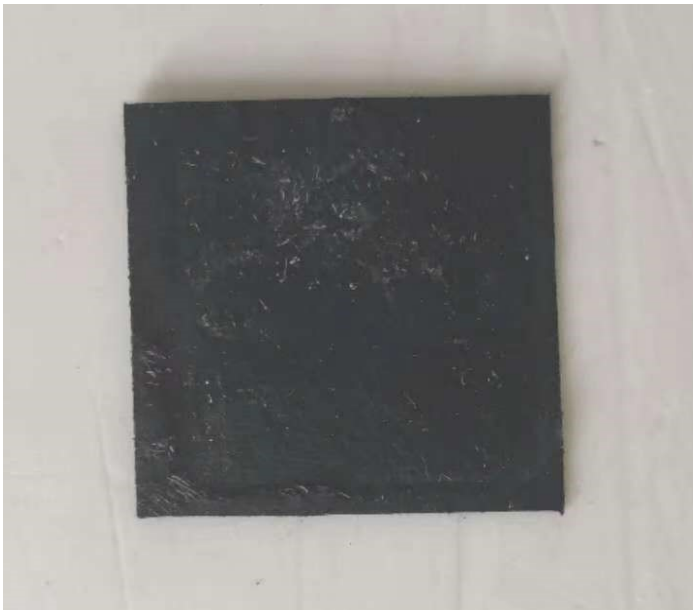

Figure S13. GDE after 10h reaction in 1M KOH (carbonate formation on the surface)

Table S7. Summary of the performances of recent Ni-based SACs for the CO_2RR toward CO

catalysts	FE_{CO}(%)	j_{CO}(mA/cm^2)	Potential (V)	Electrolyte	Cell system
Ni–SAs–NC[1]	75	31	-0.96	0.5M $KHCO_3$	H-cell
NiSA@N3-C[2]	96.0	18.87	-0.83	0.5M $KHCO_3$	H-cell
Ni-SAC@NC[3]	95	5.7	−0.60	0.5M $KHCO_3$	H-cell
Ni–N–C[4]	94	~10	−0.60	0.5M $KHCO_3$	H-cell
Ni@NCNTs[5]	99.1	~13	−0.90	0.5M $KHCO_3$	H-cell
Ni–Zn–N–V[6]	99	17	−0.80	0.5M $KHCO_3$	H-cell

Ni/NC[7]	96.5	12.6	-0.90	0.1M $KHCO_3$	H-cell
Ni3-NC-1000[8]	98.2	6.86	−0.9	0.1M $KHCO_3$	H-cell
Ni-HPNCF[9]	90	49.6	-1	0.5M $KHCO_3$	H-cell
Ni-N/OMC-1[10]	~100	27	-1	0.5M $KHCO_3$	H-cell
Ni-NUK-900[11]	94	3.4	−0.73	0.5M $KHCO_3$	H-cell
Ni–N–C[12]	91.2	10.8	−0.9	0.5M $KHCO_3$	H-cell
This work	95	46.88	-0.73	0.5M $KHCO_3$	H-cell

Table S8. The binding energies of the Ni/NC-0 and Ni/NC-2:1 to the reaction intermediates

	Ni/NC-0	**Ni/NC-2:1**
△G1/eV	-0.0478	-0.2262
△G2/eV	0.7796	0.7530
△G3/eV	0.1795	0.1871
△G4/eV	-0.9112	-0.7140

[1] W. Wang, C. Cao, K. Wang, T. Zhou, Boosting CO_2 electroreduction to CO with abundant nickel single atom active sites, Inorg. Chem. Front. 8 (2021) 2542–2548. https://doi.org/10.1039/D1QI00126D.

[2] L. Qiu, S. Shen, C. Ma, C. Lv, X. Guo, H. Jiang, Z. Liu, W. Qiao, L. Ling, J. Wang, Controllable fabrication of atomic dispersed low-coordination nickel-nitrogen sites for highly

efficient electrocatalytic CO_2 reduction, Chemical Engineering Journal 440 (2022) 135956. https://doi.org/10.1016/j.cej.2022.135956.

[3] X. Wang, S. Ding, T. Yue, Y. Zhu, M. Fang, X. Li, G. Xiao, Y. Zhu, L. Dai, Universal domino reaction strategy for mass production of single-atom metal-nitrogen catalysts for boosting CO_2 electroreduction, Nano Energy 82 (2021) 105689. https://doi.org/10.1016/j.nanoen.2020.105689.

[4] Z. Li, D. He, X. Yan, S. Dai, S. Younan, Z. Ke, X. Pan, X. Xiao, H. Wu, J. Gu, Size-Dependent Nickel-Based Electrocatalysts for Selective CO_2 Reduction, Angewandte Chemie International Edition 59 (2020) 18572–18577. https://doi.org/10.1002/anie.202000318.

[5] Y. Li, X.F. Lu, S. Xi, D. Luan, X. Wang, X.W. (David) Lou, Synthesis of N-Doped Highly Graphitic Carbon Urchin-Like Hollow Structures Loaded with Single-Ni Atoms towards Efficient CO_2 Electroreduction, Angewandte Chemie International Edition 61 (2022) e202201491. https://doi.org/10.1002/anie.202201491.

[6] S. Shen, C. Han, B. Wang, Y. Wang, Self-Supported Nickel Single Atoms Overwhelming the Concomitant Nickel Nanoparticles Enable Efficient and Selective CO_2 Electroreduction, Adv. Mater. Interfaces 8 (2021) 2101542. https://doi.org/10.1002/admi.202101542.

[7] G. Hwa Jeong, Y. Chuan Tan, J. Tae Song, G.-Y. Lee, H. Jin Lee, J. Lim, H. Young Jeong, S. Won, J. Oh, S. Ouk Kim, Synthetic multiscale design of nanostructured Ni single atom catalyst for superior CO_2 electroreduction, Chemical Engineering Journal 426 (2021) 131063. https://doi.org/10.1016/j.cej.2021.131063.

[8] G.-D. Park, S. Sirisomboonchai, K. Norinaga, Facile Synthesis and Insight of Atomically Dispersed Ni Catalyst on N-doped Carbonized Lignin for Highly Efficient Electrochemical CO_2 Reduction to CO, ChemSusChem (2023) e202300530. https://doi.org/10.1002/cssc.202300530.

[9] I. Song, Y. Eom, M.A. P, D.H. Hong, M. Balamurugan, R. Boppella, D.H. Kim, T.K. Kim, Geometric and Electronic Structural Engineering of Isolated Ni Single Atoms for a Highly Efficient CO_2 Electroreduction, Small n/a (n.d.) 2300049. https://doi.org/10.1002/smll.202300049.

[10] Q.-X. Li, D.-H. Si, W. Lin, Y.-B. Wang, H.-J. Zhu, Y.-B. Huang, R. Cao, Highly efficient electroreduction of CO_2 by defect single-atomic Ni-N_3 sites anchored on ordered micro-macroporous carbons, Sci. China Chem. (2022). https://doi.org/10.1007/s11426-022-1263-5.

[11] X. Chen, W. Liu, Y. Sun, T. Tan, C. Du, Y. Li, KOH-Enabled Axial-Oxygen Coordinated Ni Single-Atom Catalyst for Efficient Electrocatalytic CO_2 Reduction, Small Methods 7 (2023) 2201311. https://doi.org/10.1002/smtd.202201311.

[12] C.-Z. Yuan, K. Liang, X.-M. Xia, Z.K. Yang, Y.-F. Jiang, T. Zhao, C. Lin, T.-Y. Cheang, S.-L. Zhong, A.-W. Xu, Powerful CO_2 electroreduction performance with N–carbon doped with single Ni atoms, Catal. Sci. Technol. 9 (2019) 3669–3674. https://doi.org/10.1039/C9CY00363K.